The Astrophysical Journal, 591:1248–1256, 2003 July 10

MODELING THE SUN'S LARGE-SCALE MAGNETIC FIELD DURING THE MAUNDER MINIMUM

Y.-M. Wang and N. R. Sheeley, Jr.
Code 7672, E. O. Hulburt Center for Space Research, US Naval Research Laboratory, Washington, DC 20375-5352;
ywang@yucca.nrl.navy.mil, sheeley@spruce.nrl.navy.mil
Received 2003 March 5; accepted 2003 March 20

ABSTRACT

We use a flux transport model to simulate the evolution of the Sun's magnetic dipole moment, polar fields, and open flux under Maunder minimum conditions. Even when the rate of active region emergence is taken to be a factor of ~30 smaller than in recent solar cycles, regular polarity oscillations of the axial dipole and polar fields can be maintained if the speed of the poleward surface flow is reduced from ~20 to ~10 m s^{-1} and the source flux emerges at very low latitudes (~10°). The axial dipole is then found to have an amplitude of the order of 0.5 G, as compared with ~4 G during solar cycle 21. The strength of the radial interplanetary field component at Earth is estimated to be in the range ~0.3–0.7 nT, about a factor of 7 lower than contemporary values. We discuss the implications of these weak fields for our understanding of geomagnetic activity and cosmic-ray modulation during the Maunder minimum.

Subject headings: interplanetary medium — solar-terrestrial relations — Sun: activity — Sun: corona — Sun: magnetic fields — Sun: photosphere

1. INTRODUCTION

In a previous paper (Wang, Lean, & Sheeley 2002a), we simulated the evolution of the Sun's large-scale magnetic field during solar cycles 13–22 (1888–1997). The model included the effect of emerging flux and its subsequent transport over the solar surface by differential rotation, supergranular convection, and a poleward bulk flow. When the flux eruption rates were scaled according to the observed sunspot numbers and the meridional flow speed was fixed, we found that the polar fields built up during the more active cycles were too strong to be reversed during the less active ones. Regular polarity reversals were obtained only if the flow rate was assumed to be positively correlated with the cycle amplitude. The inferred poleward velocities varied from ~15 m s^{-1} for cycles 14, 16, and 20 to ~27.5 m s^{-1} for cycle 19; the corresponding maximum yearly sunspot numbers for these cycles range from ~60 to ~200.

During the period of the Maunder minimum (1645–1715), sunspot numbers peaked at values even lower than those recorded during present-day activity minima (see Eddy 1976, 1983; Ribes & Nesme-Ribes 1993; Hoyt & Schatten 1996; Beer, Tobias, & Weiss 1998; Cliver, Boriakoff, & Bounar 1998; Letfus 2000). We now ask whether, by suitably adjusting the meridional flow speed, we can maintain the polarity reversals even with such a dramatic reduction in the source flux. If so, how strong are the derived polar and interplanetary fields, and how do they vary with time? How much open and closed magnetic flux remains during intervals when no activity is present at all?

In a related investigation, Mackay (2003) has presented simulations of idealized "grand minima" using a flux transport model. Mackay's approach differs substantially from ours, however, in that he fixes the flow amplitude and does not require that the polar fields reverse their sign during every cycle.

The organization of this paper is as follows. We begin with a brief discussion of the sunspot data used to constrain our simulations of the Maunder minimum (§ 2). After outlining our basic model and procedure (§ 3), we show how the evolution of the Sun's axial dipole and polar fields depends on the meridional flow velocity and on the source latitudes (§ 4) and then illustrate how the large-scale magnetic field might have evolved during the Maunder minimum (§ 5). Our results and their implications are discussed in § 6.

2. SUNSPOT ACTIVITY DURING THE MAUNDER MINIMUM

Eddy (1976) has given an estimate of the mean sunspot number R_Z for each year between 1650 and 1715. According to his Table 1, R_Z attained peak values of 3 in 1652, 4 in 1660, 10 in 1676, 11 in 1684, 6 in 1695, and 18 in 1705. In contrast, the maximum and minimum values of R_Z during solar cycle 21 were 155.4 (1979) and 12.6 (1976).

Another measure of the relative level of sunspot activity during the Maunder minimum is provided by the group sunspot numbers R_G that Hoyt & Schatten (1998) inferred for the years 1610–1995. The index R_G is derived solely from the number of sunspot groups observed and is less noisy than the standard Wolf index R_Z, which also counts individual spots. In assessing the completeness of the Maunder minimum data, Hoyt & Schatten (1996) estimated that observations were made on roughly $\frac{2}{3}$ of the days between 1645 and 1715. As pointed out by Letfus (2000), East Asian records indicate as many as 14 naked-eye sunspots between 1647 and 1709; of these, nine occurred during years (1647, 1648, 1650, 1659, 1665, and 1666) for which R_G was assigned a value of 0.0. Thus, the R_G series probably somewhat underestimates the actual number of sunspot groups during the Maunder minimum.

Between 1645 and 1715, the yearly averaged R_G peaked at values of 4.0 in 1652, 2.0 in 1660, 1.8 in 1676, 1.4 in 1684, and 5.5 in 1705. In general, these numbers are smaller than the corresponding R_Z estimates of Eddy (1976), given above. During the period immediately preceding and following the Maunder minimum, the largest values of R_G were 76.8 (1639) and 33.9 (1719), respectively. For comparison, $R_G = 155.7$ during the 1979 activity maximum.

Measurements of the ^{10}Be concentration (Beer et al. 1998) and butterfly diagram reconstructions (Ribes & Nesme-Ribes 1993) suggest that the solar cycle continued to operate throughout the Maunder minimum. From the extant sunspot data, we are unable to ascertain the durations of the individual cycles or even their exact number. Beer et al. (1998) use the minima and maxima of the ^{10}Be concentration in a Greenland ice core to infer the dates of the corresponding activity maxima and minima; their Table I shows six cycles between 1649 and 1714, with minimum-to-minimum durations ranging from $\sim$9 to $\sim$13 yr and averaging about 11 yr. However, the phases of the ^{10}Be-derived cycles are in poor agreement with the R_G and R_Z time series.

Measurements made at the Paris Observatory and described by Ribes & Nesme-Ribes (1993) show the great majority of sunspots during 1666–1712 occurring in the southern hemisphere and near the equator, at an average latitude of $\sim 10^\circ$ south. During the cycle immediately following the Maunder minimum, however, the sunspots were distributed more or less uniformly between latitudes $\sim 25^\circ$ north and $\sim 25^\circ$ south (see Fig. 6 in Ribes & Nesme-Ribes 1993).

3. METHOD

3.1. *Equations and Definitions*

Let r denote heliocentric radius, L heliographic latitude, ϕ Carrington longitude, and t time. The radially oriented photospheric field $B_r(R_\odot, L, \phi, t)$ is assumed to obey the equation

$$\frac{\partial B_r}{\partial t} = -\omega(L)\frac{\partial B_r}{\partial \phi} + \kappa \nabla_\perp^2 B_r - \frac{1}{R_\odot \cos L}\frac{\partial}{\partial L}[v(L) B_r \cos L] + S(L, \phi, t) , \quad (1)$$

where $\nabla_\perp^2$ denotes the L and ϕ components of the Laplacian, $\omega(L)$ is the synodic rotation rate of the photospheric plasma, κ is the diffusion constant associated with the supergranular convection (Leighton 1964), $v(L)$ is the poleward flow velocity, and $S(L, \phi, t)$ is the source term. After specifying the transport parameters and the sources of emerging flux during the Maunder minimum (see § 3.2), we integrate equation (1) for an assumed initial photospheric field using the numerical code of Sheeley, DeVore, & Boris (1985).

To characterize the large-scale magnetic field, we define the following quantities. The total photospheric flux is expressed as a surface-averaged field strength,

$$B_{\rm tot}(t) = \frac{1}{4\pi}\int |B_r(R_\odot, L, \phi, t)|\, d\Omega , \quad (2)$$

where the integral is over all solid angles Ω. The average fields in the north ($L > 60^\circ$) and south ($L < -60^\circ$) polar caps are given by

$$B_n(t) = \frac{\int B_r(R_\odot, L, \phi, t)\, d\Omega_{L>+60^\circ}}{\int d\Omega_{L>+60^\circ}} , \quad (3)$$

$$B_s(t) = \frac{\int B_r(R_\odot, L, \phi, t)\, d\Omega_{L<-60^\circ}}{\int d\Omega_{L<-60^\circ}} . \quad (4)$$

The strengths of the axial and equatorial dipole components of the photospheric field are defined as $D_{\rm ax}(t)$ and $D_{\rm eq}(t) = (H_1^2 + H_2^2)^{1/2}$, where

$$D_{\rm ax}(t) = \frac{3}{4\pi}\int B_r(R_\odot, L, \phi, t)\sin L\, d\Omega , \quad (5)$$

$$H_1(t) = \frac{3}{4\pi}\int B_r(R_\odot, L, \phi, t)\cos L\cos\phi\, d\Omega , \quad (6)$$

$$H_2(t) = \frac{3}{4\pi}\int B_r(R_\odot, L, \phi, t)\cos L\sin\phi\, d\Omega . \quad (7)$$

We extrapolate the photospheric field into the corona by assuming that the current-free condition $\nabla \times \boldsymbol{B} = 0$ holds out to a "source surface" at $r = R_{\rm ss} = 2.5\ R_\odot$, where the tangential components of the field are set to zero (Schatten, Wilcox, & Ness 1969). The total open flux is then given by

$$\Phi_{\rm open}(t) = R_{\rm ss}^2 \int |B_r(R_{\rm ss}, L, \phi, t)|\, d\Omega . \quad (8)$$

Since the open flux is uniformly distributed in L and ϕ at $r = r_{\rm E} = 1$ AU (Balogh et al. 1995), the radial interplanetary magnetic field (IMF) strength $B_{\rm E}$ at Earth is related to $\Phi_{\rm open}$ through

$$B_{\rm E}(t) = \frac{\Phi_{\rm open}}{4\pi r_{\rm E}^2} . \quad (9)$$

Because of the rapid falloff of higher order magnetic multipoles between $r = R_\odot$ and $r = R_{\rm ss}$, $\Phi_{\rm open}$ and $B_{\rm E}$ depend principally on the dipole ($l = 1$) and quadrupole ($l = 2$) components of the photospheric field (see Wang, Lean, & Sheeley 2000a).

3.2. *Specification of the Model Parameters and Source Term*

Based on the positions of $\sim$100 sunspots that were observed over successive days during the period 1666–1719, Ribes & Nesme-Ribes (1993) deduced that the photospheric rotation was slower and more differential in the Maunder minimum than at the present day. A steeper rotational gradient would tend to hasten the decay of the Sun's nonaxisymmetric field component, without significantly affecting the evolution of the axial dipole and polar fields. In view of the uncertainties inherent in deriving a rotation profile from relatively sparse sunspot data (with conflicting results being obtained by Ribes & Nesme-Ribes 1993, Eddy, Gilman, & Trotter 1977, and Abarbanell & Wöhl 1981), we continue to employ the standard Snodgrass (1983) formula $\omega(L) = 13.38 - 2.30\sin^2 L - 1.62\sin^4 L$ deg day^{-1}. Because we have no observational or physical grounds for supposing that the supergranular cell sizes and lifetimes were different during the Maunder minimum, we set $\kappa = 500$ km^2 s^{-1}, the value that we obtained by modeling the large-scale field during solar cycle 21 (Wang, Sheeley, & Lean 2002b). For simplicity, we also assume that the latitude dependence of the poleward flow is the same as inferred in the latter study,

$$|v(L)| = v_m \cos^2 L \sin^{0.025}|L| ; \quad (10)$$

however, the flow amplitude v_m is now taken to be a free parameter that may vary from cycle to cycle (as in Wang et al. 2002a).

In investigating the effect of randomized source longitudes on the solar cycle evolution of the large-scale field, we have previously represented $S(L, \phi, t)$ by 600 idealized bipolar magnetic regions (BMRs), each having a total flux

of 5×10^{22} Mx and a longitudinal pole separation of 15° (Wang & Sheeley 2003). The resulting values of $D_{ax}(t)$, $D_{eq}(t)$, $B_n(t)$, $B_s(t)$, and $B_E(t)$ were found to be similar to their observed magnitudes during cycle 21. For our Maunder minimum simulations, we again employ doublet sources having strengths of 5×10^{22} Mx and pole separations of 15° but scale their number downward in proportion to the cycle amplitudes, as measured by the maximum values of R_G and R_Z during each cycle. As in Wang & Sheeley (2003), the east-west and north-south polarity orientations of the BMRs are assumed to obey the usual Hale-Joy laws, with the angle γ between their axes and the east-west line increasing with latitude according to $\sin\gamma = 0.6 \sin|L|$ (see Wang & Sheeley 1991).

For definiteness, we suppose that eight 11 yr activity cycles occurred in the interval from 1635 through 1722. During the "deep minimum" (1646–1700), the characteristic sunspot number amplitude is taken to be $R_{MM} = 5$, which represents a rough average between the peak R_G values of Hoyt & Schatten (1998) and the corresponding R_Z estimates of Eddy (1976). In each of the five deep minimum cycles, we then deposit a total of $(R_{MM}/R_{21})600 \simeq (5/155)600 \simeq 20$ BMRs; here $R_{21} \simeq 155$ is the maximum value of R_G and R_Z during cycle 21. The corresponding BMR totals for the "outer" cycles are $(77/155)600 \simeq 300$ (1635–1645), $(12/155)600 \simeq 45$ (1701–1711), and $(34/155)600 \simeq 130$ (1712–1722). Within each cycle, the deposition rate is modulated so that it peaks ~4 yr after the start of the cycle. The BMRs are distributed randomly over a 10° wide band centered about a latitude L_0. To limit the number of adjustable parameters, we take L_0 to be independent of t during any given cycle (so that it represents a cycle-averaged source latitude), while allowing its value to vary from one cycle to another. A random number generator is also used to assign a longitude and, unless otherwise noted, a hemisphere (north or south) to each BMR.

4. EFFECT OF VARYING THE FLOW SPEED AND AVERAGE SOURCE LATITUDE

The main constraint that we impose on our simulations is that the large-scale magnetic field should reverse its polarity during every cycle. This assumption implies that the amplitude of $D_{ax}(t)$ during the deep Maunder minimum (1646–1700) must be well below contemporary values, since the available source flux (20 BMRs per cycle) would otherwise be insufficient to reverse the axial dipole component. Conversely, the photospheric field at the start of the "precursor cycle" in 1635 cannot be too weak; otherwise, the deposition of 300 BMRs over the next 11 yr would lead to an overly strong axial dipole at the onset of the deep minimum. The implied correlation between the cycle amplitude and the dipole strength during the preceding sunspot minimum is consistent with conventional dynamo models, where the active region flux is generated by winding up the preexisting poloidal field.

We begin by considering possible scenarios for the precursor cycle (1635–1645). In the absence of relevant observations, we arbitrarily suppose that the polar fields in 1635 had the same polarity as in 1976 but were $\frac{2}{3}$ as strong (see Wang & Sheeley 1995); thus,

$$B_r(R_\odot, L, \phi, 0) = 8\ \mathrm{G} \sin^7 L\ . \qquad (11)$$

The 300 BMRs that we have allotted to this cycle are deposited in succession at randomized longitudes and at an average latitude $L_0 = \pm 15°$. Figure 1 shows the evolution of the axial dipole component and polar fields for three choices of the poleward flow amplitude v_m. The initial values of D_{ax}, B_n, and B_s are 2.7, 5.2, and −5.2 G, respectively. When $v_m = 15\ \mathrm{m\ s^{-1}}$ (Fig. 1*a*), the corresponding values at the end of the 11 yr cycle are −1.7, −4.3, and 4.5 G, somewhat less than but comparable to the initial strengths. If the flow speed is increased by only 2.5 m s^{-1} to 17.5 m s^{-1}, however, D_{ax}, B_n, and B_s fall precipitously to −0.4, −1.6, and 1.7 G, respectively (Fig. 1*b*). Finally, when $v_m = 20\ \mathrm{m\ s^{-1}}$ (Fig. 1*c*), the fields end up not only much weaker than at the start of the cycle but with the same polarity as before, having undergone two changes of sign.

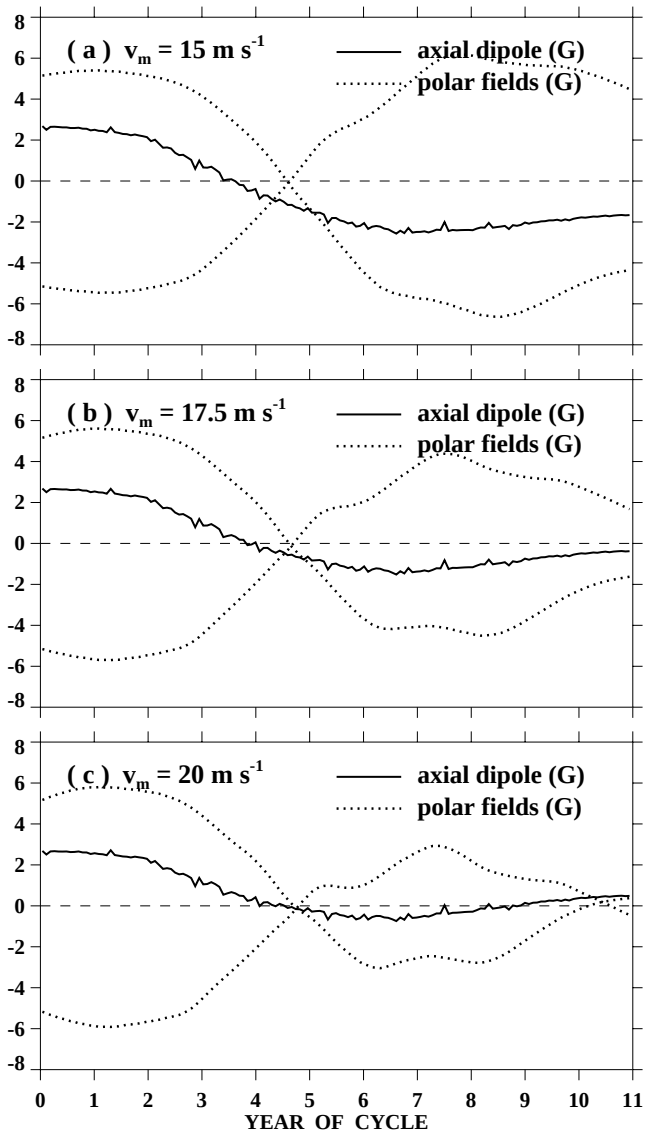

FIG. 1.—Effect of different poleward flow speeds on the evolution of the Sun's axial dipole component and polar fields during the precursor cycle (1635–1645): $v_m =$ (*a*) 15, (*b*) 17.5, and (*c*) 20 m s^{-1}. Solid curves represent $D_{ax}(t)$ (in G); dotted curves denote $B_n(t)$ and $B_s(t)$ (in G), the average fields poleward of $L = +60°$ and $-60°$, respectively. In each case, 300 BMRs were deposited sequentially at random longitudes and over a 10° wide band centered at latitude $L_0 = \pm 15°$; the initial photospheric field was taken to be of the form $8\ \mathrm{G} \sin^7 L$.

These results may be understood as follows. To cancel and reverse the polar fields, a net quantity of trailing polarity flux must be transported from the source regions to the poles. A fast low-latitude flow inhibits the diffusion of leader flux across the equator and sweeps both polarities poleward, resulting in a comparatively small change in the polar fields and axial dipole component. For the assumed source rate and initial field, Figure 1*b* indicates that a flow of amplitude $v_m = 17.5$ m s^{-1} carries so much leading polarity flux to the poles that the axial dipole component is only just able to reverse its sign. The nonmonotonic behavior of $B_n(t)$, $B_s(t)$, and $D_{ax}(t)$ seen after activity maximum in all three simulations is a consequence of the equatorward shift of the leader flux, which arrives at the poles systematically later in the cycle than the trailing polarity flux. The overshooting caused by the delayed mutual cancellation is particularly dramatic when v_m is increased to 20 m s^{-1} (Fig. 1*c*); in this case, both the axial dipole and the polar fields undergo a second polarity reversal near the end of the cycle.

The main point to be derived from Figure 1 is that the final strengths of the axial dipole and polar fields are extremely sensitive to the meridional flow speed. Thus, small cycle-to-cycle fluctuations in v_m, if not compensated for by (larger amplitude) changes in the source rate, can cause $|D_{ax}|$ to decrease or increase abruptly from one activity minimum to the next. Figure 1 suggests that the required velocity fluctuations may be as small as ± 2.5 m s^{-1}.

Focusing now on a typical low-amplitude cycle during the deep Maunder minimum, we reduce the number of BMRs from 300 to 20 and consider the effect of varying the average source latitude and the flow rate. The initial photospheric field is taken to be $B_r(R_\odot, L, \phi, 0) = 1.5$ G $\sin^7 L$, a factor of 5.3 weaker than in the simulations of Figure 1. Figure 2 illustrates the behavior of $D_{ax}(t)$, $B_n(t)$, and $B_s(t)$ for $v_m = 7.5$ m s^{-1} and three different choices of L_0. When the BMRs are deposited at a mean latitude of $\pm 15°$ (Fig. 2*a*), a substantial amount of leading polarity flux is carried to the poles along with the trailing polarity flux, so that the axial dipole and polar fields end up only about half as strong as at the start of the cycle. When $L_0 = \pm 10°$ (Fig. 2*b*), a greater fraction of the leader flux is able to diffuse across the equator, and the initial and final values of D_{ax} are equal in magnitude but opposite in sign. Depositing the sources at $L_0 = \pm 5°$ (Fig. 2*c*) does not produce any further increase in the axial dipole strength, however, because BMRs that emerge so close to the equator have very small axial tilts and north-south dipole moments.

Figure 3 illustrates the effect of varying the flow speed while keeping L_0 fixed at $\pm 10°$. We see that decreasing v_m from 12.5 m s^{-1} (Fig. 3*a*) to 7.5 m s^{-1} (Fig. 3*b*) more than doubles the final value of D_{ax}. However, further reducing the flow speed to 2.5 m s^{-1} (Fig. 3*c*) produces no additional increase in the axial dipole strength, while significantly delaying the reversal of the polar fields. The value of $|D_{ax}|$ no longer grows for very small v_m because of the latitude-dependent nature of the flow, which attains its peak speed at $L = \pm 6\overset{\circ}{.}4$, according to equation (10). On the one hand, the poleward flow tends to weaken D_{ax} by impeding the diffusion of leader flux across the equator; at the same time, however, it acts to separate the poles of the BMRs and thus to increase their north-south dipole moments at low latitudes, an effect that disappears as $v_m \to 0$ (see Figs. 4 and 5 in Wang & Sheeley 1991).

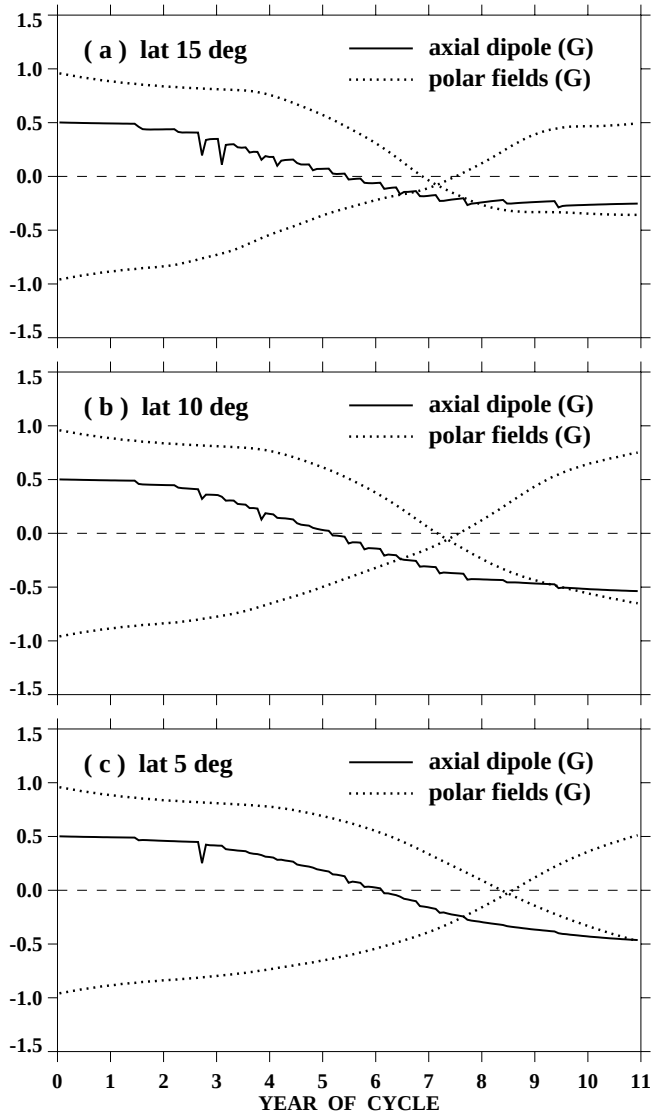

FIG. 2.—Effect of variations in the average source latitude on the evolution of the axial dipole and polar fields during a low-amplitude cycle: (*a*) $|L_0| = 15°$; (*b*) $|L_0| = 10°$; (*c*) $|L_0| = 5°$. In each case, 20 BMRs were deposited sequentially at random longitudes and over a 10° wide band centered at the given L_0; the flow amplitude was fixed at $v_m = 7.5$ m s^{-1}, and the initial photospheric field was set equal to 1.5 G $\sin^7 L$.

These exploratory calculations suggest that, in order for polarity oscillations to be maintained from cycle to cycle, an average, long-term correlation must exist between the source rate, the axial dipole strength at the start of the cycle, and the meridional flow speed. On the other hand, a small fluctuation in the flow rate that is not balanced by an appropriate increase or decrease in the source rate can lead to a large change in the axial dipole strength from one cycle to the next, thus triggering or ending a grand minimum.

5. MAUNDER MINIMUM SIMULATIONS

To provide an illustrative simulation of the entire period from 1635 through 1722, we again adopt equation (11) as our initial photospheric field and assign to the eight 11 yr cycles the values of $|L_0|$ and v_m listed in Table 1. The flow amplitude drops from 17.5 m s^{-1} during 1635–1645 to

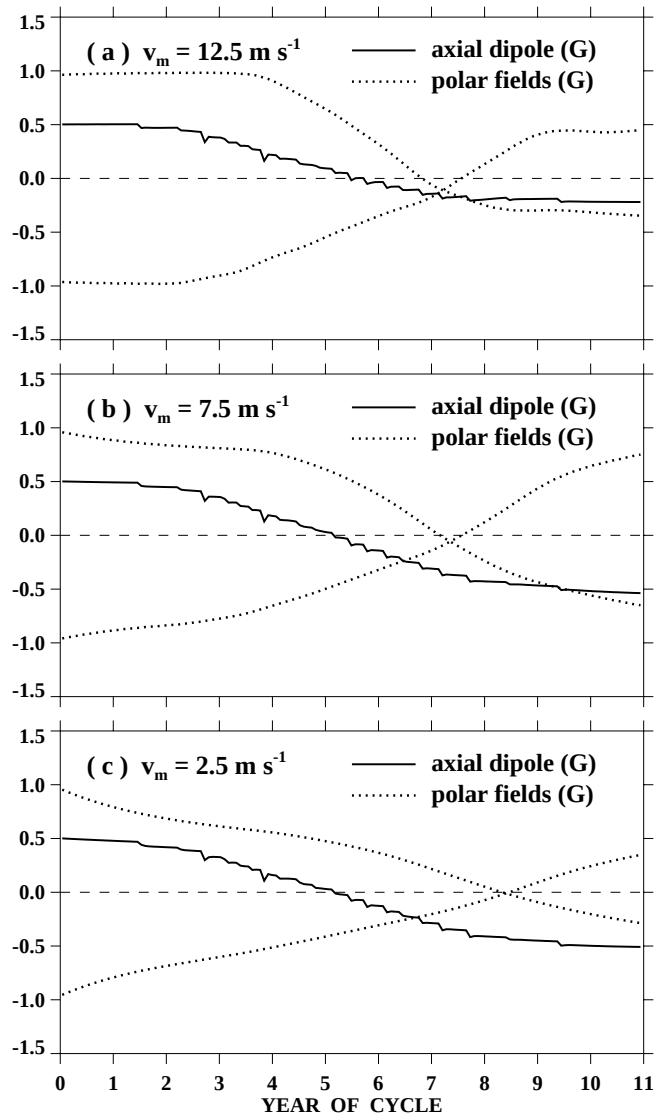

FIG. 3.—Effect of the poleward flow speed on the evolution of the axial dipole and polar fields during a low-amplitude cycle: $v_m = (a)$ 12.5, (b) 7.5, and (c) 2.5 m s^{-1}. In each case, 20 BMRs were deposited sequentially at random longitudes and over a 10° wide band centered at $L_0 = \pm 10°$; the initial photospheric field was set equal to 1.5 G $\sin^7 L$.

7.5 m s^{-1} during 1657–1700, while the average source latitude simultaneously decreases from $|L_0| = 15°$ to 10°.

Figure 4 shows a latitude-time plot of the photospheric field over the entire 88 yr period, constructed by longitudinally averaging maps of $B_r(R_\odot, L, \phi, t)$ taken at successive 27.3 day intervals. Especially striking are the sudden weakening of the polar fields after the 1635–1645 precursor cycle and their rapid regeneration in the final two cycles. The individual BMRs are clearly visible during the low-amplitude cycles; the long, vertical streaks mark the trajectories of the trailing polarity flux as it streams poleward and reverses the weak polar fields.

TABLE 1

PARAMETERS OF MAUNDER MINIMUM SIMULATION

Cycle	Number of BMRs	Source Latitude $\|L_0\|$ (deg)	Flow Amplitude v_m (m s^{-1})
1635–1645	300	15	17.5
1646–1656	20	12.5	10
1657–1667	20	10	7.5
1668–1678	20	10	7.5
1679–1689	20	10	7.5
1690–1700	20	10	7.5
1701–1711	45	10	10
1712–1722	130	12.5	12.5

In Figure 5, we plot the time evolution of $B_{\rm tot}$, B_n, B_s, $D_{\rm ax}$, $D_{\rm eq}$, and $B_{\rm E}$. The total photospheric flux is roughly correlated with the source rate (indicated by the dotted lines in Fig. 5*a*), falling by a factor of the order of 7 between the maxima of the first and second cycles. During a typical low-amplitude cycle, $B_{\rm tot}(t)$ (which omits the contribution of ephemeral regions) ranges from ~0.25 G at activity minimum to ~2 G at activity maximum. In those years when no sources are deposited, the main contribution to $B_{\rm tot}(t)$ comes from the weak polar fields.

During the minima of the low-amplitude cycles, the axial dipole component $|D_{\rm ax}(t)|$ peaks at ~0.5 G (Fig. 5*b*), while the equatorial dipole and near-Earth radial IMF strengths fall to 0 G and ~0.3 nT, respectively (Fig. 5*c*). The polar cap fields attain their maximum strengths of ~0.7–0.9 G during the rising phase of the cycle, while both $D_{\rm eq}(t)$ and $B_{\rm E}(t)$ peak around midcycle, when their values approach, respectively, ~1 G and ~0.7 nT.

The slowness of the meridional flow during the low-amplitude cycles and the consequent tendency for the polar fields to reverse well after activity maximum suggest that the actual durations of these cycles may have been longer than 11 yr (the inverse relationship between solar cycle period and flow speed is discussed by Dikpati & Charbonneau 1999, Wang et al. 2002a, and Hathaway et al. 2003). However, provided that the number of BMRs deposited per cycle remains the same, increasing the interval between one cycle minimum and the next will not change the final equilibrium value of $D_{\rm ax}$ or $B_{\rm E}$ attained at the end of the cycle.

In the above simulation, the sources were distributed randomly between the two hemispheres. However, almost all of the sunspots observed between 1666 and 1711 were located south of the equator (Ribes & Nesme-Ribes 1993). We have therefore repeated the calculation with the same sequence of sources, except that those BMRs that were earlier assigned a latitude $L > 0$ during 1646–1711 are now deposited at latitude $-L$. As may be seen from Figures 6 and 7, the effect is to make the polar field somewhat stronger in the south than in the north; also, the variation of $B_n(t)$ lags that of $B_s(t)$, since the trailing polarity flux is carried to the south pole before the leading polarity flux has had time to diffuse across the equator and reach the north pole. The final values of $B_{\rm tot}$, B_n, B_s, $D_{\rm ax}$, $D_{\rm eq}$, and $B_{\rm E}$ in 1722 are almost identical in both simulations.

The Carrington format maps in Figure 8 illustrate the distribution of the photospheric field and open flux (coronal holes) at the end of 1683, as derived from the second of the two models. A series of narrow, sheared holes has formed within the decaying BMR remnants located below the equator. Although sunspot activity has just peaked, the leader flux has not yet arrived at the north pole and the old-cycle polar hole still survives in the northern hemisphere. Figure 9 displays the corresponding flux distributions in 1689, at the end of the same low-amplitude cycle. The polar fields have reversed their sign and the new-cycle polar holes are now fully developed,

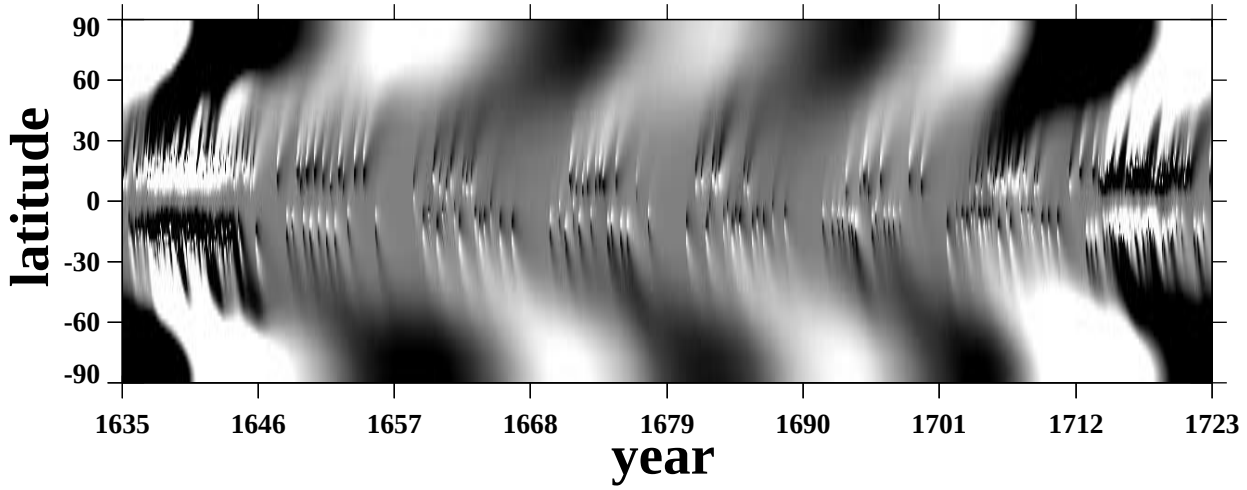

FIG. 4.—Latitude-time plot showing the evolution of the photospheric field during 1635–1722, as simulated using the parameters in Table 1. Each column of pixels represents a map of $B_r(R_\odot, L, \phi, t)$ taken at 27.3 day intervals and averaged over ϕ. Gray scale ranges from $\langle B_r \rangle_\phi < -1$ G (*black*) to $\langle B_r \rangle_\phi > +1$ G (*white*).

extending down to latitudes of 60° and below; because of the lingering presence of negative polarity flux from an earlier active region at low latitudes, the north polar hole also shows a remnant equatorward lobe.

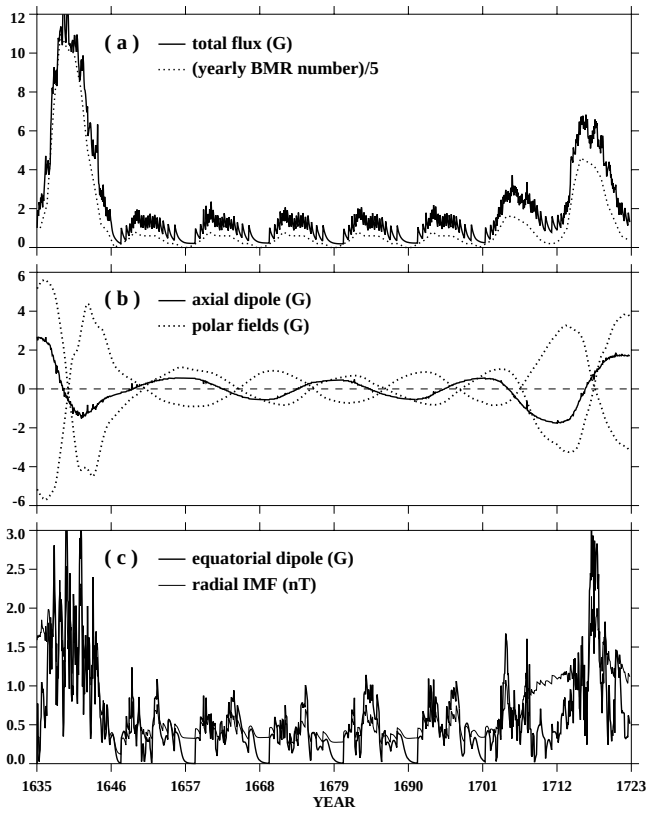

FIG. 5.—Evolution of the solar magnetic field during 1635–1722, as simulated using the parameters in Table 1 (see also Fig. 4). (*a*) Time variation of the total photospheric flux $B_{\rm tot}$ (in G), expressed as a surface-averaged field strength. Dotted lines indicate the number of BMRs deposited during each year of the cycle (or annual rate of flux emergence). (*b*) Evolution of the axial dipole component $D_{\rm ax}$ (in G) (*solid curve*) and of the average fields poleward of $L = \pm 60°$, B_n and B_s (in G) (*dotted curves*). (*c*) Time variation of the equatorial dipole strength $D_{\rm eq}$ (in G) (*thick curve*) and of the total open flux $B_{\rm E}$ (in nT), expressed as a radial IMF strength at 1 AU (*thin curve*).

6. SUMMARY AND DISCUSSION

In our reconstruction of the Sun's large-scale magnetic field during the Maunder minimum, we have assumed that polarity oscillations persisted throughout this period, that the rate of flux emergence scaled as the observed sunspot numbers, and that the active regions continued to obey the standard Hale-Joy laws. These assumptions allow surprisingly stringent constraints to be placed on the meridional flow velocity, on the source latitudes, and on the strength of the large-scale fields. Our conclusions may be summarized as follows:

1. A correlation exists between the cycle amplitude, the strength of the axial dipole component at the start of the cycle, and the poleward flow speed. A large reduction in the source rate, such as occurred when the Sun entered the Maunder minimum, must be accompanied by a corresponding decrease in $|D_{\rm ax}|$ and v_m; otherwise, polarity reversals would no longer take place.

2. Small cycle-to-cycle fluctuations in the flow amplitude, if not offset by corresponding changes in the source rate, can cause the axial dipole and polar fields to weaken or strengthen suddenly from one activity minimum to the next. Our simulations suggest that an increase of v_m by only a few meters per second above its "equilibrium" value might have been sufficient to initiate the Maunder minimum by reducing $|D_{\rm ax}|$ to extremely low values. The origin of the assumed fluctuations in the meridional flow speed is unknown to us.

3. The flow velocity and average source latitude during the deep Maunder minimum are inferred to be $v_m \sim 7.5$–10 m s^{-1} and $|L_0| \sim 10°$, respectively. These values promote the separation of polarities into opposite hemispheres (allowing the leader flux to diffuse across the equator) and thereby maximize the amplitude of the surviving polarity oscillations. The low flow speeds suggest that the periods of the low-amplitude cycles may have been longer than 11 yr.

4. With the source rate taken to be a factor of ~30 smaller than in solar cycle 21, the large-scale magnetic field during the deep Maunder minimum is found to be 5–10 times weaker than in the present day. The predicted amplitude of the axial dipole component is ~0.5 G, as compared

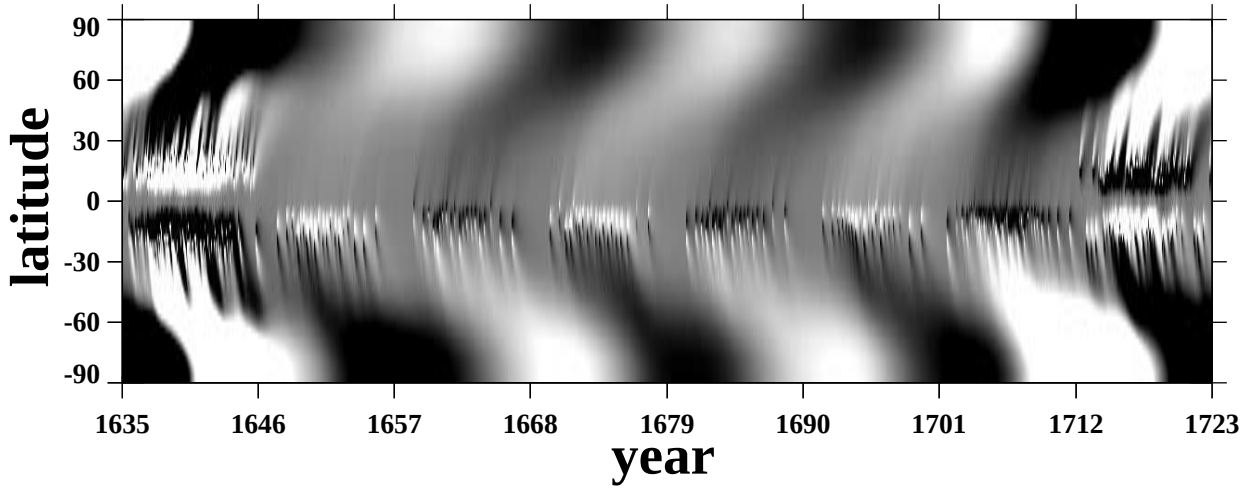

FIG. 6.—Same as Fig. 4, except that all BMRs during 1646–1711 have been deposited in the south rather than being distributed randomly between the two hemispheres.

with ~4 G during cycle 21. The near-Earth radial IMF strength ranged from ~0.3 nT at activity minimum to ~0.7 nT around the middle of each cycle, when the equatorial dipole reached its peak strength of ~1 G.

The derived field strengths clearly depend on the assumed rate of flux emergence during the Maunder minimum. If the number of BMRs were doubled, for example, D_{ax}, B_n, and B_s would likewise double, as would the value of B_E at cycle minimum; with the sources randomly distributed in longitude, the equatorial dipole strength D_{eq} would increase by a factor of $\sim 2^{1/2}$ (see Wang & Sheeley 2003). Based on the frequency and times of occurrence of moderate-latitude auroral events, Letfus (2000) suggests that the majority of active regions during 1645–1700 did not contain sunspots, in which case the source rate could be much greater than supposed here. However, strong active region fields would presumably still have been detectable as bright faculae near the solar limb, whereas a report by Cassini (cited in Ribes & Nesme-Ribes 1993) implies that white-light faculae were uncommon during the deep Maunder minimum. Our model also omits ephemeral regions, which may provide a major

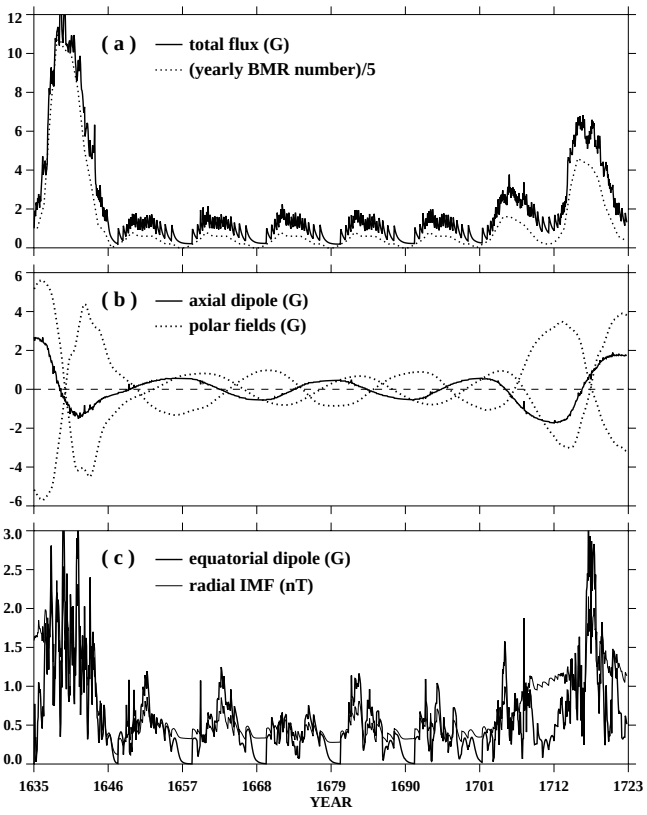

FIG. 7.—Same as Fig. 5, except that all BMRs during 1646–1711 have been deposited in the southern hemisphere. The corresponding latitude-time plot is displayed in Fig. 6.

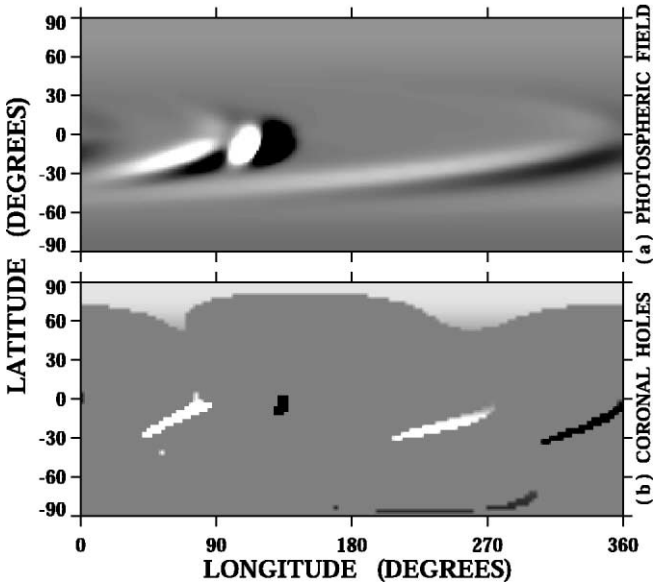

FIG. 8.—Carrington format (latitude-longitude) maps recorded at the end of 1683 (near cycle maximum), from the simulation of Figs. 6 and 7. (*a*) Photospheric field. Gray scale ranges between $B_r < -5$ G (*black*) and $B_r > +5$ G (*white*). (*b*) Open field regions (coronal holes). Gray scale ranges between $B_{open} < -1$ G (*black*) and $B_{open} > +1$ G (*white*); closed field areas are neutral gray.

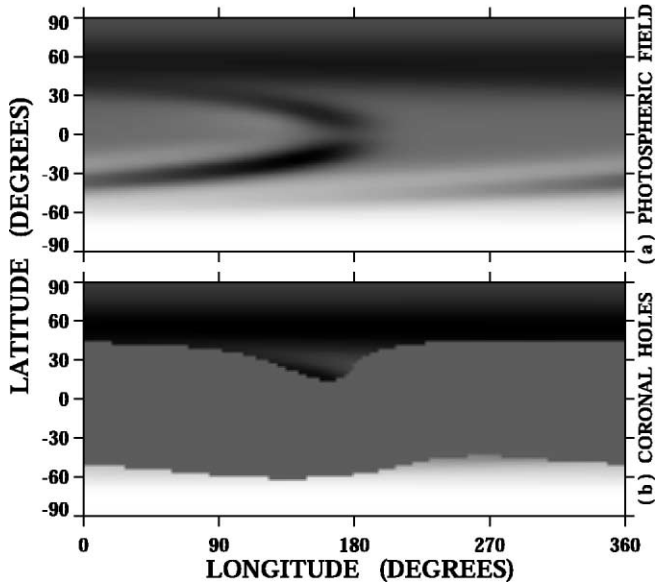

FIG. 9.—Same as Fig. 8, but recorded at the end of 1689 (near cycle minimum).

contribution to the total photospheric flux at cycle minimum, when our simulations give $B_{\rm tot} \simeq 0.25$ G. On the other hand, because their pole separations are very small and their axes tend to be randomly oriented, such bipoles are not expected to contribute significantly to the Sun's dipole moment and open flux (see Wang & Sheeley 1991).

In calculating the radial IMF strength, we have set the source surface radius $R_{\rm ss}$ equal to 2.5 $R_\odot$, the value inferred from present-day coronal and heliospheric observations. Suess (1979) speculated that the entire coronal field may have been open during the Maunder minimum, which would correspond to placing the source surface at the photosphere. The result would be to increase $B_{\rm E}$ by less than a factor of 2 at cycle minimum (when the photospheric flux is concentrated toward the poles) but by as much as a factor of $\sim$10 when active regions are present. However, we see no physical justification for supposing that strong bipoles during the Maunder minimum should have consisted entirely of open flux.

If the IMF was indeed $\sim$7 times weaker during the deep Maunder minimum than at the present time, as our simulations indicate, this prediction needs to be reconciled with auroral and ^{10}Be records. Figure 4 in Eddy (1976) shows the number of European auroral sightings falling steeply (by a factor of $\sim$10) between the 1620s and the latter half of that century. Nevertheless, during 1645–1700, an average of 3 aurorae were seen annually at geomagnetic latitudes below 55° north, most of them in years for which $R_G = 0.0$ (see Fig. 3 in Letfus 2000). It is probable that the majority of these moderate-latitude aurorae were associated with coronal mass ejections (CMEs) and that active regions were present through most of the Maunder minimum (as we have assumed in our simulations), even if their sunspots were missed by observers. The remaining events may have been triggered by solar wind streams from open field regions (coronal holes). As illustrated by Figure 9, low-latitude holes and polar hole extensions may greatly outlive the active regions near which they form; in the absence of new activity, their lifetimes are determined by the meridional flow timescale $\tau_f \sim R_\odot/v_m$ (see Wang, Sheeley, & Lean 2000b), which is as long as $\sim$3 yr when $v_m \sim 7.5$ m s^{-1}. In addition, the concentration of activity near the equator during the Maunder minimum would have served to direct the coronal hole wind toward Earth. On the other hand, the geo-effectiveness of these wind streams would have been counteracted by the reduction in the IMF strength.

According to Lockwood, Stamper, & Wild (1999), the power transferred from the solar wind to the Earth's magnetosphere scales as

$$P_w \propto n_w^{0.28} v_w^{1.56} B_{\rm E}^{0.77} , \qquad (12)$$

where n_w and v_w are, respectively, the density and velocity of the wind plasma. The weakening of the photospheric field during the Maunder minimum would have reduced the coronal heating rate and thus both n_w and the solar wind mass flux $n_w v_w$ (Suess 1979). Whether v_w was also significantly lower is less clear; if the energy and mass flux decreased at the same rate, there would have been no change in the energy per proton and thus in the wind speed. In the contemporary solar wind, v_w is mainly a function of the flux tube expansion rate rather than of the coronal field strength (see Wang & Sheeley 1990); the coronal hole expansion geometry would have been similar during the Maunder minimum. In any case, if $B_{\rm E}$ was a factor of $\sim$7 lower in the Maunder minimum than in cycle 21, then P_w was reduced by at least a factor of $\sim$4.5, as was the geomagnetic index $aa \propto P_w$. For comparison, Cliver et al. (1998) derived a reduction factor of $\sim$3.4 from a linear regression relating 11 yr averages of the *aa*-index and sunspot number.

Terrestrial ^{10}Be is produced by interactions of galactic cosmic rays with atmospheric oxygen and nitrogen. The cosmic-ray flux is in turn modulated by solar activity–induced changes in the IMF and solar wind (see, e.g., Jokipii & Marti 1986). Beer et al. (1998) found that the ^{10}Be concentration was higher during the Maunder minimum than in the present, as expected if the IMF strength was reduced and more cosmic rays impinged on the Earth's atmosphere. (The reduction in the size of the heliosphere due to the lower ram pressure of the solar wind would also have contributed to the increase in the cosmic-ray flux.) More surprisingly, the ^{10}Be abundance continued to exhibit $\sim$11 yr variations, with an amplitude comparable to that measured for recent solar cycles. If our model predictions are correct, this result implies that a heliospheric field only $\sim\frac{1}{7}$ as strong as the present one would still provide a significant barrier to the cosmic rays that give rise to ^{10}Be. Such magnetic fields (with $B_{\rm E}$ ranging from $\sim$0.3 to $\sim$0.7 nT instead of from $\sim$2 to $\sim$5 nT) would act to deflect mainly cosmic rays with energies below 1 GeV, while at the same time allowing a much greater flux of these particles to penetrate into the inner heliosphere. We may speculate that the amplitude of the ^{10}Be oscillations did not decrease appreciably during the Maunder minimum because the peak of the cosmic-ray spectrum shifted to lower energies. In addition, occasional CME events would have produced significant short-term enhancements in the IMF strength around cycle maximum. An alternative possibility, suggested by Lal (1987), is that the ^{10}Be oscillations are caused primarily not by cosmic rays but by climate-related changes in the ^{10}Be fallout rate.

This study has raised a number of questions about the physical nature of the Maunder minimum. Although we

have suggested that fluctuations in the Sun's global meridional circulation may be responsible for long-term variations in the solar cycle, we do not know why such fluctuations should occur or how they are related to the rate of magnetic flux emergence. In addition, our conclusion that the large-scale coronal field and IMF were much weaker during the Maunder minimum may have important implications for our understanding of the contemporary heliosphere. That auroral events were observed throughout the deep Maunder minimum, for example, suggests a rather weak dependence of the solar wind speed on the strength of the coronal field. The continued solar cycle modulation of the ^{10}Be abundance is particularly surprising, given our prediction that the IMF strength was down by a factor of 5–10; reconciling these two results may shed light on the interstellar cosmic-ray spectrum and on the propagation of cosmic rays through the heliosphere.

We are indebted to J. Lean and J. R. Jokipii for valuable comments. This work was funded by NASA and the Office of Naval Research.

REFERENCES

Abarbanell, C., & Wöhl, H. 1981, Sol. Phys., 70, 197
Balogh, A., Smith, E. J., Tsurutani, B. T., Southwood, D. J., Forsyth, R. J., & Horbury, T. S. 1995, Science, 268, 1007
Beer, J., Tobias, S., & Weiss, N. 1998, Sol. Phys., 181, 237
Cliver, E. W., Boriakoff, V., & Bounar, K. H. 1998, Geophys. Res. Lett., 25, 897
Dikpati, M., & Charbonneau, P. 1999, ApJ, 518, 508
Eddy, J. A. 1976, Science, 192, 1189
———. 1983, Sol. Phys., 89, 195
Eddy, J. A., Gilman, P. A., & Trotter, D. E. 1977, Science, 198, 824
Hathaway, D. H., Nandy, D., Wilson, R. M., & Reichmann, E. J. 2003, ApJ, 589, 665
Hoyt, D. V., & Schatten, K. H. 1996, Sol. Phys., 165, 181
———. 1998, Sol. Phys., 181, 491
Jokipii, J. R., & Marti, K. 1986, in The Galaxy and the Solar System, ed. R. Smoluchowski, J. N. Bahcall, & M. S. Matthews (Tucson: Univ. Arizona Press), 116
Lal, D. 1987, Geophys. Res. Lett., 14, 785
Leighton, R. B. 1964, ApJ, 140, 1547
Letfus, V. 2000, Sol. Phys., 197, 203
Lockwood, M., Stamper, R., & Wild, M. N. 1999, Nature, 399, 437
Mackay, D. H. 2003, Sol. Phys., 213, 173
Ribes, J. C., & Nesme-Ribes, E. 1993, A&A, 276, 549
Schatten, K. H., Wilcox, J. M., & Ness, N. F. 1969, Sol. Phys., 6, 442
Sheeley, N. R., Jr., DeVore, C. R., & Boris, J. P. 1985, Sol. Phys., 98, 219
Snodgrass, H. B. 1983, ApJ, 270, 288
Suess, S. T. 1979, Planet. Space Sci., 27, 1001
Wang, Y.-M., Lean, J., & Sheeley, N. R., Jr. 2000a, Geophys. Res. Lett., 27, 505
———. 2002a, ApJ, 577, L53
Wang, Y.-M., & Sheeley, N. R., Jr. 1990, ApJ, 355, 726
———. 1991, ApJ, 375, 761
———. 1995, ApJ, 447, L143
———. 2003, ApJ, 590, 1111
Wang, Y.-M., Sheeley, N. R., Jr., & Lean, J. 2000b, Geophys. Res. Lett., 27, 621
———. 2002b, ApJ, 580, 1188